Relationship Between Applied Stress and Hydrogen-Related Fracture Behavior in Martensitic Steel

Yasunari Takeda, Takashi Yonemura, Yuji Momotani, Akinobu Shibata, and Nobuhiro Tsuji

Abstract

In the present study, a relationship between the applied stress and the hydrogen-related fracture behavior in an 8Ni-0.1C martensitic steel was investigated by means of constant loading tensile tests under various applied stresses ranging from 400 to 1000 MPa. The time to fracture in hydrogen charged specimens increased from 0.5 to 30.5 s with decreasing the applied stress from 1000 to 400 MPa. Area fractions of brittle fracture surfaces, especially that of intergranular fracture surface, increased as the applied stress decreased. Orientation analysis using EBSD showed that micro-cracks observed in the vicinity of the main crack initiated along prior austenite grain boundaries regardless of the applied stress. The hydrogen-related fracture processes under various applied stresses were reconstructed by fracture surface topography analysis and the results indicated that intergranular fracture was dominant under the lower applied stress, while the fracture mode changed from intergranular fracture to quasi-cleavage fracture with progress of crack propagation under the higher applied stress.

Introduction

Hydrogen embrittlement is the phenomenon that materials become very brittle due to the existence of hydrogen. Since high strength steels, especially martensitic steels, show high susceptibility to hydrogen embrittlement, this is one of the serious issues for practical applications of high strength steels. There are mainly two fracture modes in hydrogen embrittlement of martensitic steels: intergranular fracture and quasi-cleavage fracture. Previous studies [1–5] reported that hydrogen-related intergranular fracture occurred along prior austenite grain boundaries. Momotani et al. proposed that hydrogen accumulated at prior austenite grain boundaries during deformation, resulting in the intergranular fracture [6]. Quasi-cleavage fracture occurs inside prior austenite grains but not along typical cleavage planes. Nagao et al. observed the microstructure beneath the hydrogen-induced quasi-cleavage fracture surface in martensitic steels [7]. Their results suggested that the quasi-cleavage fracture path was along lath boundaries. Shibata et al. found through a crystallographic orientation analysis that the quasi-cleavage fracture occurred on {011} plane [8–10]. To reveal the distinct condition that controls the fracture mode in hydrogen embrittlement is one of the important keys for understanding the mechanism of hydrogen embrittlement. It has been reported that the fraction of intergranular fracture increased with increasing hydrogen content [3], impurities content [11, 12] or decreasing the tempering temperature [2]. Deformation conditions, such as strain rate, stress concentration factor and applied stress, are also the important factors which affect hydrogen-related fracture behavior. Momotani et al. reported that the fraction of brittle fracture surfaces significantly

Y. Takeda (✉) · T. Yonemura · Y. Momotani · A. Shibata N. Tsuji
Department of Materials Science and Engineering, Kyoto University, Kyoto, Japan
e-mail: takeda.yasunari.62v@st.kyoto-u.ac.jp

T. Yonemura
e-mail: yonemura.takashi@tsujilab.mtl.kyoto-u.ac.jp

Y. Momotani
e-mail: momotani.yuji@tsujilab.mtl.kyoto-u.ac.jp

A. Shibata
e-mail: shibata.akinobu.5x@kyoto-u.ac.jp

N. Tsuji
e-mail: nobuhiro-tsuji@mtl.kyoto-u.ac.jp

A. Shibata · N. Tsuji
Elements Strategy Initiative for Structural Materials, Kyoto University, Kyoto, Japan

increased with decreasing the strain rate [6]. Wang et al. carried out slow strain rate tensile tests using the specimens with various stress concentration factors, and found that the intergranular fracture region increased as the stress concentration factor increased [3]. However, the effect of the applied stress on hydrogen-related fracture modes in martensitic steel has not been quantitatively clarified in detail. In the present study, the relationship between the applied stress and the hydrogen-related fracture mode in martensitic steels was investigated by means of constant loading tensile tests under various applied stresses.

Experimental Procedure

An 8Ni-0.1C steel was used in the present study. The chemical composition of the steel is shown in Table 1. A cast ingot of the steel was homogenized at 1100 °C for 9 h followed by air cooling. The homogenized ingot was cold-rolled to a thickness of 1.7 mm. Then the sheet was austenitized at 1000 °C for 30 min followed by ice brine quenching and sub-zero cooling in liquid nitrogen to obtain a fully martensitic structure. Specimens for constant loading tensile tests were cut from the heat-treated sheets and mechanically polished on both surfaces until the final thickness of 1 mm was reached to remove the decarburized layers formed during the heat treatments. The gauge length, width, and thickness of the specimen were 10 mm, 5 mm, and 1 mm, respectively. After polishing the surfaces of the specimen with a 3 μm diamond suspension, the specimen was cathodically pre-charged with hydrogen in a 3% NaCl aqueous solution including 3 g L^{-1} NH_4SCN at a current density of 3 A m^{-2} for 24 h. The diffusible hydrogen content after hydrogen pre-charging measured by a thermal desorption analysis was 1.72 wt. ppm. After the hydrogen pre-charging, constant loading tensile tests were carried out under the various applied stresses ranging from 400 to 1000 MPa at ambient temperature. To prevent a desorption of hydrogen, hydrogen charging at a current density of 3 A m^{-2} was continued during the constant loading tensile tests. Fracture surfaces were observed using scanning electron microscopy (SEM, JEOL: JSM-7800F). To reveal microstructural features of hydrogen-related cracks, electron backscattering diffraction (EBSD) analysis was carried out using SEM (JEOL: JSM-7100F). Hydrogen-related fracture process during the constant loading tensile test was simulated by fracture surface topography analysis (FRASTA). A FRASTA technique is a procedure for reconstructing a fracture process in microscopic level [13]. There are three
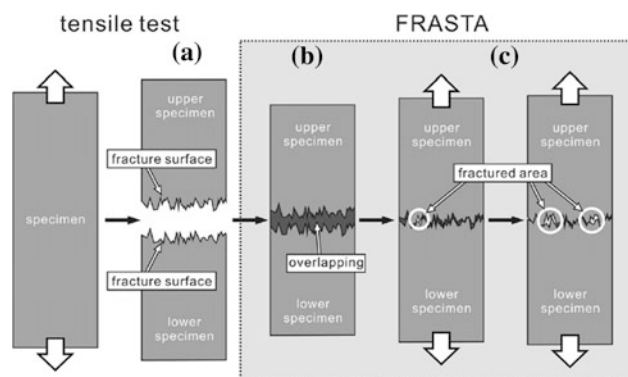

Fig. 1 Schematic illustration showing the method of fracture surface topography analysis (FRASTA) [14]

steps in the FRASTA method: (1) obtain topographic maps of conjugate area in opposing fracture surfaces, (2) overlap the two topographic maps computationally until there is no gap between them and (3) increase the relative distance between the two topographic maps. A schematic illustration of FRASTA method is shown in Fig. 1 [14].

Results and Discussion

Figure 2 shows an optical microscopy image of the heat-treated specimen. The microstructure exhibits a typical lath martensite structure consisting of laths, blocks, packets and prior austenite grains. The stress-strain curve of the uncharged specimen at ambient temperature at a strain rate
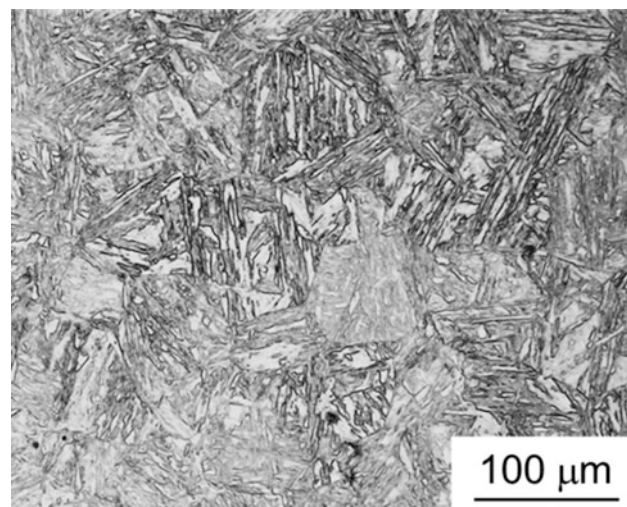

Fig. 2 Optical microscopy image of the heat-treated specimen

Table 1 Chemical composition of the steel used in the present study (wt%)

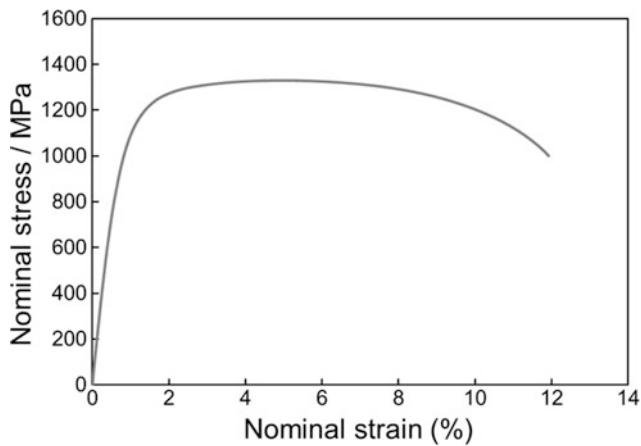| C	Ni	Mn	Al	Si	P	S	Fe
0.116	7.94	0.01	0.033	0.005	0.001	0.0015	Bal.

Fig. 3 Nominal stress–nominal strain curve of the uncharged specimen at ambient temperature at a strain rate of 8.3×10^{-6} s^{-1}
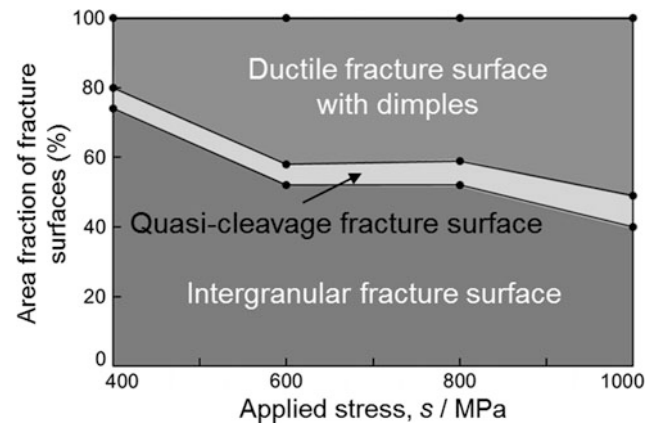

Fig. 6 Area fractions of different fracture surfaces after the constant loading tensile tests under various applied stresses
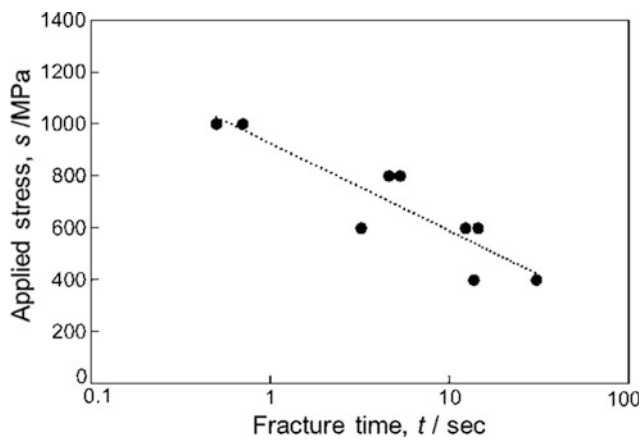

Fig. 4 Relationship between the applied stress and the fracture time in the constant loading tensile tests

of 8.3×10^{-6} s^{-1} is presented in Fig. 3. The 0.2% proof stress and ultimate tensile strength measured from the stress-strain curve are 928 MPa and 1287 MPa, respectively.

Figure 4 shows the relationship between the applied stress and the fracture time in the constant loading tensile tests. While the applied stress of 1000 MPa is higher than the 0.2% proof stress, the other applied stresses ranging from 400 to 800 MPa are within elastic deformation region of the uncharged specimen. It can be found from Fig. 4 that the fracture time increased from 0.5 to 30.5 s with decreasing the applied stress from 1000 to 400 MPa. Figure 5 are SEM images showing typical fracture surfaces after the constant loading tensile test (applied stress = 1000 MPa). Intergranular fracture surface, quasi-cleavage fracture surface and ductile fracture surface with dimple patterns were observed in Fig. 5a–c, respectively. Figure 6 summarizes the relationship between the area fractions of various types of fracture surfaces and the applied stresses. As the applied stress decreased, the area fraction of brittle fracture surfaces,
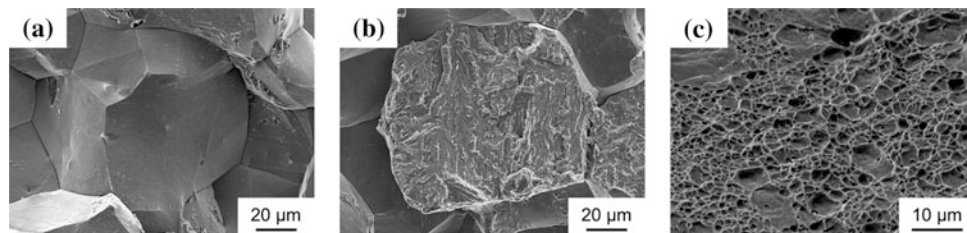

Fig. 5 SEM images showing typical fracture surfaces observed after the constant loading tensile tests (applied stress = 1000 MPa); a intergranular fracture surface, b quasi-cleavage fracture surface and c ductile fracture surface with dimples

Fig. 7 **a**, **b** SEM images and **c**, **d** corresponding EBSD orientation maps showing the micro-cracks observed in the vicinity of the main cracks in the specimens tested under the applied stresses of **a**, **c** 400 MPa and **b**, **d** 1000 MPa, respectively. Packet boundaries and prior austenite grain boundaries are drawn by white lines and white broken lines, respectively
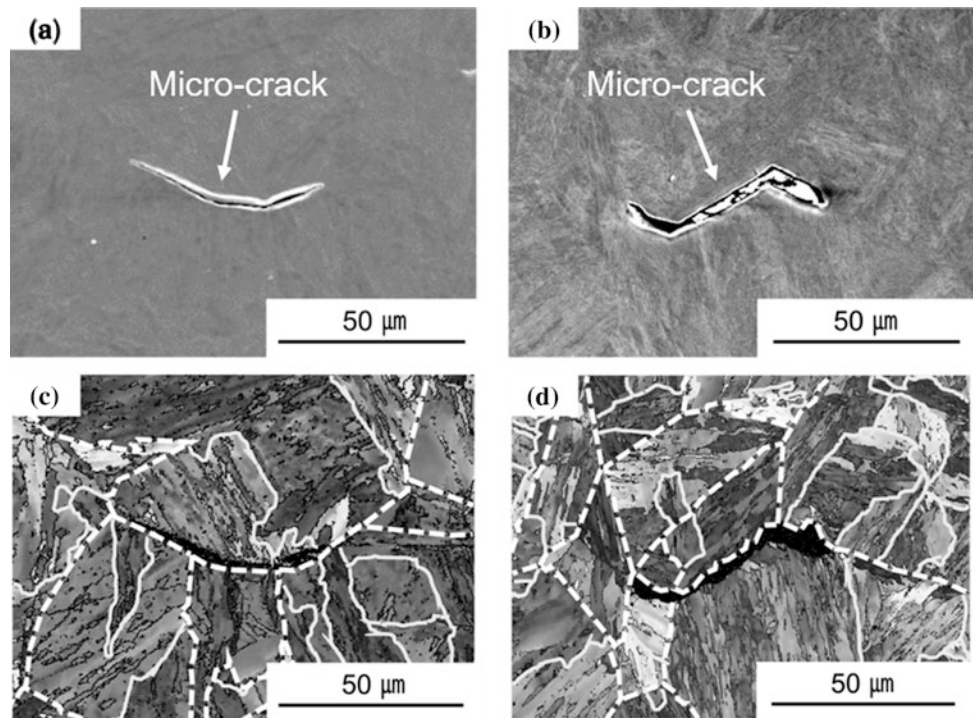
particularly that of intergranular fracture surfaces, significantly increased. The results shown in Figs. 4 and 6 indicate that the higher applied stress accelerated hydrogen-related fracture, but decreased the area fraction of brittle fracture surfaces.

Figure 7 are SEM images showing micro-cracks observed in the vicinity of the main cracks in the specimens tested under the applied stresses of (a) 400 and (b) 1000 MPa, respectively. Figure 7c, d shows EBSD orientation maps of the same regions as Fig. 7a, b. In these figures, packet boundaries and prior austenite grain boundaries identified by crystallographic orientation analysis are drawn in white lines and white broken lines, respectively. It is obvious from these figures that the micro-cracks formed along prior austenite grain boundaries in both cases. The results indicate that the hydrogen-related fracture initiated along prior austenite grain boundaries regardless of the applied stress.

Figure 8 summarizes changes in the fraction of each fracture surface under the applied stresses of (a) 400 MPa and (b) 1000 MPa, respectively, evaluated by FRASTA. The horizontal axis shows the distance (L) between the conjugate

topography maps of fracture surfaces. L is defined as 0 at which the first cracking occurs in the specimen. Under the applied stress of 400 MPa (Fig. 8a), intergranular fracture mainly occurred at the early stages of fracture and the fraction of ductile fracture surface with dimples increased as the fracture proceeded. It was reported that hydrogen accumulated at prior austenite grain boundaries during deformation [6]. Therefore, the results suggest that under the lower applied stress, such as a stress in elastic region, hydrogen accumulation at prior austenite grain boundaries around the crack tip is necessary for the crack propagation. When the applied stress was 1000 MPa (Fig. 8b), on the other hand, not only intergranular fracture but also quasi-cleavage fracture and ductile fracture occurred at the early stages of fracture. It is considered that under the higher applied stress, such as a stress higher than the 0.2% proof stress, cracks can propagate easily even in transgranular manner once micro-cracks form. Therefore, the fracture time decreased and the fraction of transgranular fracture surfaces, such as quasi-cleavage fracture surface and ductile fracture surface, increased as the applied stress increased.
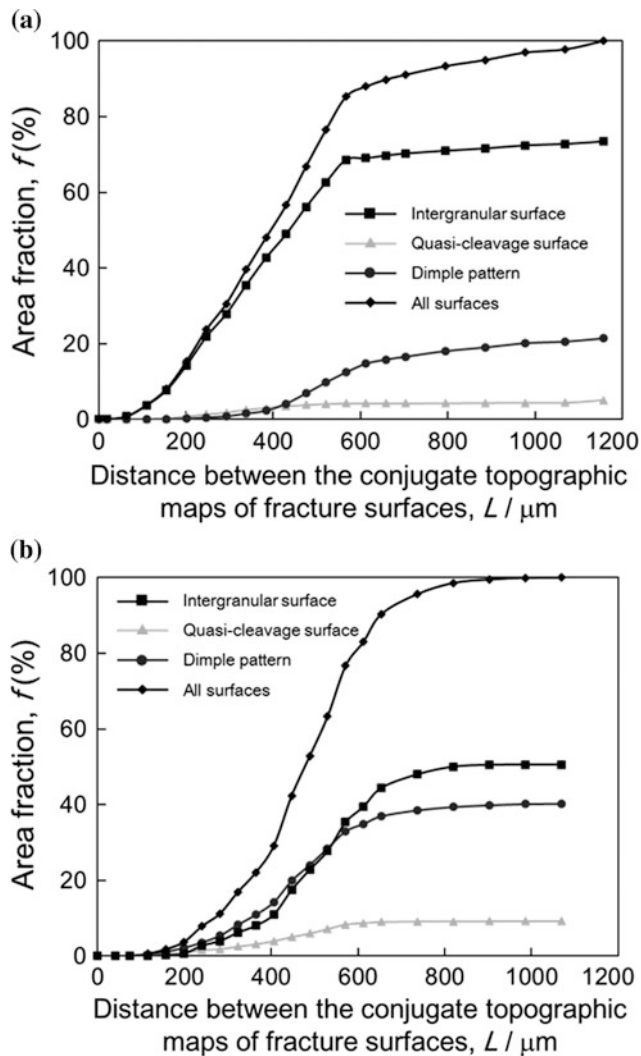
Fig. 8 Changes in fraction of each fracture mode under the applied stress of **a** 400 MPa and **b** 1000 MPa summarized as a function of the distance between the conjugate topography maps of fracture surfaces

Summary

In the present study, constant loading tensile tests under various applied stresses were carried out to reveal the relationship between the applied stress and the hydrogen-related fracture behavior. The main results obtained are as follows:

- The fracture time increased with decreasing the applied stress. As the applied stress decreased, the fractions of brittle fracture surfaces, especially that of intergranular fracture surfaces, increased. The results indicated that the hydrogen-related fracture was accelerated with increasing the applied stress, while the fracture mode became more brittle as the applied stress decreased.
- According to the EBSD orientation analysis, it was found that hydrogen-related cracking initiated along prior grain boundaries regardless of the applied stress.
- Hydrogen-related fracture processes during the constant loading tensile tests were reconstructed by FRASTA. Under the lower applied stress, the crack propagation proceeded mainly by intergranular fracture. Under the higher applied stress, on the other hand, the crack propagation occurred not only by intergranular fracture but also quasi-cleavage fracture and ductile fracture.

References

1. Banerji SK, McMahon C, Feng HC (1978) Intergranular fracture in 4340-type steels: effects of impurities and hydrogen. Metall Mater Trans A 9(2):237–247
2. Craig BD, Krauss G (1980) The structure of tempered martensite and its susceptibility to hydrogen stress cracking. Metall Trans A 11(11):1799–1808
3. Wang M, Akiyama E, Tsuzaki K (2005) Effect of hydrogen and stress concentration on the notch tensile strength of AISI 4135 steel. Mater Sci Eng A 398(1):37–46
4. Wang M, Akiyama E, Tsuzaki K (2007) Effect of hydrogen on the fracture behavior of high strength steel during slow strain rate test. Corros Sci 49(11):4081–4097
5. Wang G et al (2013) Hydrogen embrittlement assessment of ultra-high strength steel 30CrMnSiNi2. Corros Sci 77:273–280
6. Momotani Y et al (2017) Effect of strain rate on hydrogen embrittlement in low-carbon martensitic steel. Int J Hydrog Energy 42(5):3371–3379
7. Nagao A et al (2012) The role of hydrogen in hydrogen embrittlement fracture of lath martensitic steel. Acta Mater 60 (13):5182–5189
8. Shibata A, Takahashi H, Tsuji N (2012) Microstructural and crystallographic features of hydrogen-related crack propagation in low carbon martensitic steel. ISIJ Int 52(2):208–212
9. Shibata A et al (2015) Characterization of hydrogen-related fracture behavior in As-quenched low-carbon martensitic steel and tempered medium-carbon martensitic steel. Metall Mater Trans A 46(12):5685–5696
10. Shibata A et al (2017) Microstructural and crystallographic features of hydrogen-related fracture in lath martensitic steels. Mater Sci Technol 33(13):1524–1532
11. Takeda Y, McMahon CJ (1981) Strain controlled vs stress controlled hydrogen induced fracture in a quenched and tempered steel. Metall Trans A 12(7):1255–1266
12. Nagumo M, Matsuda H (2002) Function of hydrogen in intergranular fracture of martensitic steels. Philos Mag A 82(17–18):3415–3425
13. Kobayashi T, Shockey DA (1987) A fractographic investigation of thermal embrittlement in cast duplex stainless steel. Metall Trans A 18(11):1941–1949
14. Shibata A et al (2017) Fracture surface topography analysis of the hydrogen-related fracture propagation process in martensitic steel. Int J Fract 205(1):73–82